Cross-sectional classification of aluminium beams subjected to fire

Cross-sectional classification of aluminium beams subjected to fire

***O. R. van der Meulen 1,2,3 ; J. Maljaars 3; F. Soetens 2,3**
1: Materials innovation institute (M2i), Mekelweg 2, Delft, the Netherlands
2: Eindhoven University of Technology, Faculty of architecture, building and planning, den Dolech 2, Eindhoven the Netherlands
3: TNO Built Environment and Geosciences, van Mourik Broekmanweg 6, Delft, the Netherlands
***corresponding author r.vandermeulen@m2i.nl**

Abstract

Fire design for aluminium alloy beams is performed using the same system of cross-sectional slenderness classes as is employed at room temperature. Identical width-over-thickness ratio limits are used to define the boundaries between the classes. These limits are known (and demonstrated) to be conservative, but may in fact be over-conservative. Especially for tempered alloys, the geometric limits may be relaxed considerably, allowing cross-sections to be upgraded in class for fire design calculations.

Introduction

The design of aluminium bending members in fire according to the European standard for structural fire design in aluminium structures [4] follows the same cross-sectional classification system as the general structural rules [3]. It also has the same geometric limits to the boundaries between the four classes. This is a conservative assumption, but is over-conservative in many instances as the resistance to local buckling increases and the required curvature to achieve redistribution of forces decreases. In this paper a study is performed to increase the geometric limits of the different cross-sectional boundaries. Failure is considered to occur through local buckling of the constituent plates only; tensile failure and lateral torsion buckling are assumed to be prevented by the choice of material and support conditions.

Cross-sectional classification

The European standard for aluminium design [3], like many other modern design standards, employs a system of cross-sectional classification for members in bending. Based on the geometry of the cross-section, expressed as the width-over-thickness ratio (b/t or β) of the constitutive plates, members are classified to be of class 1, 2, 3 or 4. The maximum allowable stress and the possibility for plastic design depend depends on the class of the cross-section.

- Class 4, the most slender class of cross-section. The conventional elastic moment $M_{0.2}$ is not reached. The maximum moment M_{rd} is reduced by an effective area approach.
- Class 3, semi compact sections. $M_{0.2}$ is reached, but not the plastic moment $\alpha_0 M_{0.2}$. The moment M_{rd} is equal to the elastic moment $M_{0.2}$.
- Class 2, compact sections. The plastic moment $\alpha_0 M_{0.2}$ is reached, but the moment decreases to fast at greater rotations to allow plastic design. M_{rd} is equal to $\alpha_0 M_{0.2}$.
- Class 1, ductile sections. The plastic moment $\alpha_0 M_{0.2}$ is reached and the moment stays above the conventional elastic moment $M_{0.2}$ for a least a certain specified rotation capacity. This allows for plastic design rules and the redistribution of forces. The normative part of [3] sets M_{rd} equal to $\alpha_0 M_{0.2}$.

α_0 is the geometric shape factor equal to the quotient of the plastic- and the elastic-section modulus. A graphical representation of the four cross-sections is given in figure 1(a).

Rotation capacity

As mentioned above, the boundary between sections of class 1 and 2 is formed by their rotation capacity. With regard to rotation capacity some ambiguity exists in nomenclature and the relevant terms are defined here therefore. The stable rotation capacity R_0 is the rotation where the calculated ultimate moment M_u is reached, decreased by, and normalized to, the elastic rotation capacity, as given in equation 1 and as demonstrated in figure 1(b).

$$R_0 \equiv \frac{\phi_u}{\phi_{0.2}} - 1. \tag{1}$$

The regular rotation capacity *R* is based on the rotation where the moment, after local-buckling has occurred, dips below the elastic moment again. This definition deviates from steel design where the plastic moment is commonly set as the boundary.

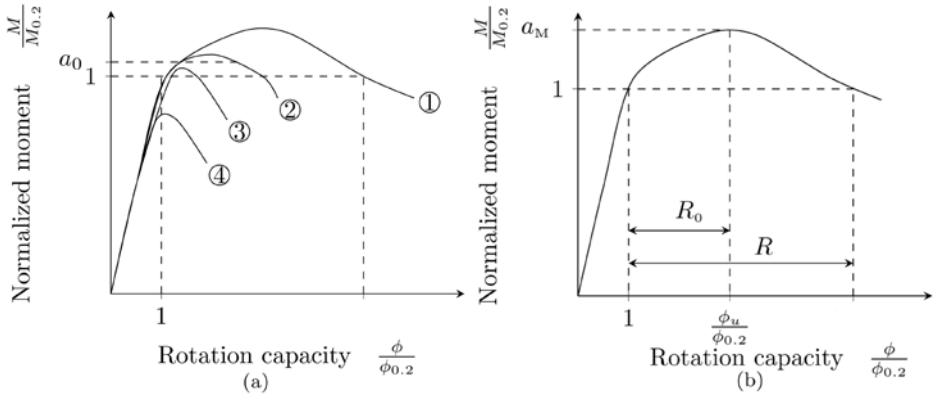

Figure 1 (a) The 4 classes of cross-section for bending members, (b) Rotation and stable rotation capacity

The question whether the stable rotation capacity R_0, or the total rotation capacity *R* should be used to define the boundary between classes 1 and 2, depends on the plastic design rules used afterwards. The actual minimum required quantity according to either limit is always somewhat arbitrary, as it depends on how inefficient a structure we are willing to consider, with regard to plastic design.

The use of the total rotation capacity *R* as a limit is most appropriate when we do not take into account strain hardening and assume a constant plastic moment. The stable rotation capacity R_0 should be used if an increase in moment past the plastic moment is considered in the subsequent strength calculations.

The Eurocode [3,4] is implicitly based on a stable rotation capacity R_0 equal to 3 [2,9], but does not consider the increase in moment past the plastic moment in the formal part of the standard. In its informative annex F however, a procedure is given which does do this. The moment used in the plastic strength calculation according to either method can be calculated trough

$$M_u = a_{M,1} W_{el} f_d, \tag{2}$$

where $a_{M,1}$ is equal to the generalized shape factor a_0 according to the formal part of the standard. The informative annex [3, annex F] sets it equal to a_5 or a_{10}, depending on the tensile ductility class of the alloy, as defined in the before mentioned informative annex.

$$a_5 = 5 - \frac{3.89 + 0.00190\, n}{a_0^{\,0.270+0.0014\, n}}. \tag{3}$$

$$a_{10} = a_0^{\,0.21 \log\left(1000\, n\right)} 10^{0.0796 - 0.0809 \log\left(\frac{n}{10}\right)}. \tag{4}$$

Equations 3 and 4 were derived by Capelli et alii[1] from a curve fit of `... numerical simulation to a wide range of cases'.

The Moment curvature relationship is a convenient tool to study the behaviour of bending members. For aluminium alloy bending members an approximation formula is given in [3, informative annex G] and [1], as:

$$\frac{\kappa}{\kappa_{0.2}} = \frac{M}{M_{0.2}} + k\left(\frac{M}{M_{0.2}}\right)^m, \text{ where } m = \frac{\log\left(\frac{10-a_{10}}{5-a_5}\right)}{\log\left(\frac{a_{10}}{a_5}\right)}, \text{ and } k = \frac{5-a_5}{a_5^m} = \frac{10-a_{10}}{a_{10}^m}. \quad (5)$$

Classes 2, 3 and 4 in fire Conditions

As already stated in the introduction, the geometrical limits to the boundaries of the four cross-sectional classes at room temperature [3], is used for the temperatures associated with fire as well [4]. This was shown to be a conservative approach by Lundberg [6] for all but one alloy tested, for which a negligible degree of un-conservativeness was found.

The influence of the temperature on the geometrical limits to the cross-sectional classes can be calculated by taking the expression for the width-over-thickness ratio (*b*/*t* or β) of the plates constituting the cross-section at room temperature:

$$\beta \equiv \frac{b}{t} = C\hat{\varepsilon}, \quad (6)$$

where *C* is an empirical constant for the given cross-sectional class limit and $\hat{\varepsilon}$ is a constant expressing the influence of the material.

$$\hat{\varepsilon} \equiv \sqrt{\frac{250}{f_{0.2}}}, \quad \text{Where } f_{0.2} \text{ is in } N/mm^2 \quad (7)$$

where, to avoid ambiguity, the Eurocode notation $\varepsilon = \hat{\varepsilon}$ is avoided. The constant 250 is a linear function of the Young's modulus *E* and `the different constants used for calculating the slenderness parameters' [6]. The value of β at elevated temperatures is denoted by β_θ and can thus be expressed by

$$\beta_\theta = \beta\frac{\hat{\varepsilon}_\theta}{\hat{\varepsilon}}, \quad (8)$$

where $\hat{\varepsilon}_\theta$ is the value of $\hat{\varepsilon}$ at elevated temperatures. The ratio between the two constants is given by [6] as

$$\frac{\hat{\varepsilon}_\theta}{\hat{\varepsilon}} = \frac{\sqrt{\frac{250k_{E,\theta}E}{70000k_{0.2,\theta}f_0}}}{\sqrt{\frac{250E}{70000f_{0.2}}}} = \sqrt{\frac{k_{E,\theta}}{k_{0.2,\theta}}}, \quad (9)$$

where $k_{E,\theta}$ and $k_{0.2,\theta}$ are constants given in [4], expressing the value of the Young's modulus and 0.2% proof stress at elevated temperatures, respectively, normalized to the value at room temperature. Combining equation 8 and 9 yields

$$\frac{\beta_\theta}{\beta} = \frac{\hat{\varepsilon}_\theta}{\hat{\varepsilon}} = \sqrt{\frac{k_{E,\theta}}{k_{0.2,\theta}}}. \quad (10)$$

Unlike steel, the ratio $\hat{\varepsilon}_\theta \,/\, \hat{\varepsilon}$ is almost invariably greater than unity for aluminium alloys, which is caused by $k_{E,\theta}$ being equal to, or larger than $k_{0.2,\theta}$,for all but one of the researched aluminium alloys. This means a cross-sectional classification system based on the room temperature derived limits to β is conservative for fire design, but may be over-conservative, as is shown in figure 2, for all alloys in [4, table 1a].

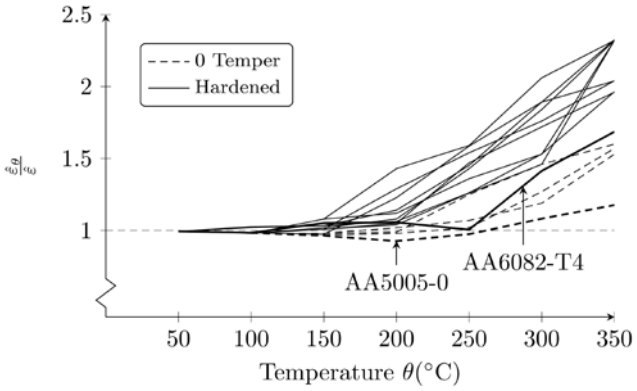

Figure 2 The stability of aluminium alloy cross-sections at elevated temperatures. Shown here are: AA3004-H34, AA5005-0, AA5005-H14, AA6082-T4, AA6063-T5, AA5052-0, AA5052-H34, AA5083-0, AA5083-H113, AA5454-0, AA5454-H32, AA6061-T6, AA6063-T6 and AA6082-T6. After: [6].

Figure 2 demonstrates the increase in stability of aluminium alloys at elevated temperatures. A notable exception is AA5005-0, which has a 7% reduction in β. While the increase in maximum β can be relatively modest for 0-temper alloys (between 8% and 46% at 300°C), a distinct increase is present for the temperature and precipitation hardened alloys (between 46% and 106%). An exception to this is AA6082-T4, which has a lower increase in β due to its high values for $f_{0.2}$ at temperatures in the range of 200 to 300°C. This is caused by the naturally aged T4 temper effectively receiving an artificial heat treatment by the fire. Given the increase in maximum β for work and artificially aged precipitation hardened alloys, it is feasible to derive a scheme to increase the geometric limits for these particular alloys at elevated temperatures. A simple and conservative approximation for these alloys as present in figure 2 is given by

$$\frac{\beta_\theta}{\beta} = \frac{\hat{\varepsilon}_\theta}{\hat{\varepsilon}} = \begin{cases} 0.16 + 0.0042\,\theta, & \text{For } 200 \le \theta \le 350^\circ\text{C} \\ 1, & \text{For } \theta < 200^\circ\text{C} \end{cases} \tag{11}$$

Class 1 in fire conditions

The geometrical limit to class 1 cross-sections at room temperature were derived from stub column compression tests such as described in [9] and [5] for square and rectangular hollow members. The ratio of the local buckling strain over the elastic strain was found to behave according to [5]

$$\frac{\varepsilon_{cr}}{\varepsilon_{0.2}} = \frac{0.905\,k}{\hat{\beta}^{C_1 + C_2\,\hat{\beta}}}, \text{ where } \hat{\beta} \equiv \frac{b}{t}\sqrt{\frac{f_{0.2}}{E}}, \tag{12}$$

where k is equal to 4, and the constants C_1 and C_2 set to 2.28 and 0.16, respectively. This is close to the analytical solution, for which *C*1 is equal to 2 and *C*2 is zero. The theoretical buckling strain is given below, which is subsequently rewritten to β.

$$\varepsilon_{cr} = \frac{k\pi^2}{12\left(1-\nu^2\right)}\left(\frac{1}{\beta}\right)^2 \Rightarrow \beta = \sqrt{\frac{\varepsilon_0}{\varepsilon_{\text{cr}}}}\sqrt{\frac{1}{\varepsilon_0}}\sqrt{\frac{k\pi^2}{12\left(1-\nu^2\right)}}. \tag{13}$$

Using equation 10, this is rewritten to a temperature dependent form, and then the quotient of the value for β at elevated temperatures to its room temperature value is obtained.

$$\beta = \sqrt{\frac{k_E(\theta)}{k_{0.2}(\theta)}}\frac{1}{\sqrt{\frac{\varepsilon_{\text{cr}}(\theta)}{\varepsilon_0(\theta)}}}\sqrt{\frac{E}{f_{0.2}}}\sqrt{\frac{k\pi^2}{12(1-\upsilon(\theta)^2)}} \Rightarrow \frac{\beta_\theta}{\beta} = \underbrace{\frac{\sqrt{1-\nu^2}}{\sqrt{1-\nu_\theta^2}}}_{\nu\text{ part}}\underbrace{\sqrt{\frac{k_{E,\theta}}{k_{0.2,\theta}}}}_{k\text{ part}}\underbrace{\sqrt{\frac{\frac{\varepsilon_{\text{cr}}}{\varepsilon_0}}{\left(\frac{\varepsilon_{\text{cr}}}{\varepsilon_0}\right)_\theta}}}_{\text{req. capacity}}. \tag{14}$$

It is noted that equation 14 represents the theoretical case for which *C*1 is equal to 2 and *C*2 is zero in equation 12. It is not possible to derive an analytical solution with the empirically derived constants C_1 and C_2 equal to 2.28 and 0.16. It is however possible to solve the equations numerically and the behaviour is very close to the analytical case.

The Poisson's ratio was assumed to be equal to 0.5 for buckling in the plastic range, especially for slender sections, this value may be too high. It is known the Poisson's ratio increases for aluminium alloys at elevated temperatures [7], but exact data is scarce and shows a significant spread. We can set the `ν-part' of equation 14 equal to unity, incurring a maximum degree of over-conservativeness of 10% based on the Poisson's ratio equal to 0.3 at room temperature and 0.5 in fire conditions. The simplification is never unconservative.

The *k*-part of equation 14 expresses the influence of the decrease in stiffness and strength at elevated temperatures relative to each other. In this part we recognize equation 10, and therefore figure 2 and equation 11 hold within the same set of conditions. The influence of the *k*-part is thus generally positive and can be described by equation 11 for temperature and precipitation hardened alloys with the exception of naturally aged varieties.

The required rotation capacity part of equation 14 describes the influence of a changing deformation demand at elevated temperatures. Class 1 alloys are different to the other classes in the sense that plastic design rules may be employed without further verification of ductility. As was described before, this was done by specifying a value for the stable rotation capacity R0. This value corresponds to a structure with a certain degree of inefficiency with regard to plastic design. As will be shown hereafter, the required amount of ductility necessary for a plastic mechanism to be able to form is highly dependent on the strain-hardening potential of the alloy through a phenomenon known as curvature localisation. This will be discussed below, but first the increasing strain hardening potential of aluminium alloys at increasing temperatures is described.

Strain hardening at elevated temperatures

The stress-strain law of round-house materials like aluminium alloys are commonly described by the well known Ramberg-Osgood equation.

$$\varepsilon = \frac{\sigma}{E} + 0.002\left(\frac{\sigma}{f_{0.2}}\right)^n, \tag{15}$$

where the exponent *n* expresses the amount of strain hardening. Work- and precipitation-hardened alloys receive their increase in 0.2% proof stress $f_{0,2}$ at the expense of their strain-hardening potential, leading to high values for *n*. In fire conditions, however, the strain-hardening potential is regained as the different tempers all tend to the annealed condition. This leads to a lower value for *n*, as was demonstrated by Maljaars[7] for both a work- and a precipitation-hardened alloy, AA5083-H111 and AA6060-T66, respectively. The value for *n* is given by

$$n = 8.8 - 0.016\theta, \qquad \text{For AA5083-H111 and } 175 \leq \theta \leq 350^{\circ}\text{C} \tag{16}$$

$$n = 19 - 0.04\theta, \qquad \text{For AA6060-T66 and } 175 \leq \theta \leq 350^{\circ}\text{C} \tag{17}$$

The room temperature values are given by [3] as equal to 5 and 16-18, respectively.

Curvature localisation

Bending members subjected to a non-constant moment, such as the simply supported beam with a single central load as depicted in figure 3(a), suffer from a phenomenon known as *`curvature localization'* [10]; which is the tendency of the bulk of the curvature to be concentrated into small regions of the beam. The effect is strongest for materials without strain hardening (*n=∞,* or elastic perfect-plastic, as steel is often modelled to behave as, within the scope of in stability calculations*)* and these theoretically localize all plastic curvature into hinges of an infinitely small linear dimension. For materials with an increasing amount of strain hardening, the effect of curvature localization decreases, and both the localization zone as the curvature are finite. This difference in behaviour, and the consequences this has for the required rotation capacity of a beam under a varying moment, is discussed below.

All plates comprising a total cross-section have a strain ε_{lb}, for which local buckling occurs, from this a certain maximum curvature κ_{lb} can be derived, at which the first plate starts to buckle. As the buckling strain ε_{lb} is independent from any material properties apart from the Poisson's ratio, it follows that this is also the case for the curvature. Assuming the Poisson's ratio equal to 0.5, which is reasonable to do because the lower limit for class 1 is well in the plastic domain and conservation of volume dictates this value for the Poisson's ratio, no material dependence remains and the buckling curvature is a geometrical property alone. It is thus possible to assume a certain maximum curvature κ_{lb} and study the effect of the material properties on the moment curvature distribution leading to this curvature. This is shown in figure 3(c) for a weak strain-hardening material with *n=30* and a strong strain-hardening with *n=5*. The ultimate moments $M_{u,n=5}$ and $M_{u,n=30}$ relative to an equal value for $M_{0.2}$, where obtained from equation 5 as a function of the assumed curvature κ_{lb} relative to the elastic curvature $\kappa_{0.2}$ value of 5 and an assumed geometrical shape factor a_0, equal to 1.5. From this figure it is clear that, as the strain hardening is increased, the maximum allowable moment goes up as well. A more dramatic effect can be seen in the curvature distribution as shown in figure 3(b), which is also derived from equation 5. Due to the effect of curvature localization, the weak strain hardening material is restricted to elastic values for most of its length, with a narrow zone of plastic behaviour only, while the strong strain hardening material is able to plastically deform along a far greater length. Integrating these curvature profiles yields the deformation of both members, along with the rotation at the supports, as shown in figure 3(d). From this figure it is apparent that the maximum rotation at the supports, and thus the (stable) rotation capacity is much larger for beams with an increased amount of strain hardening in case of a variable moment across the beam.

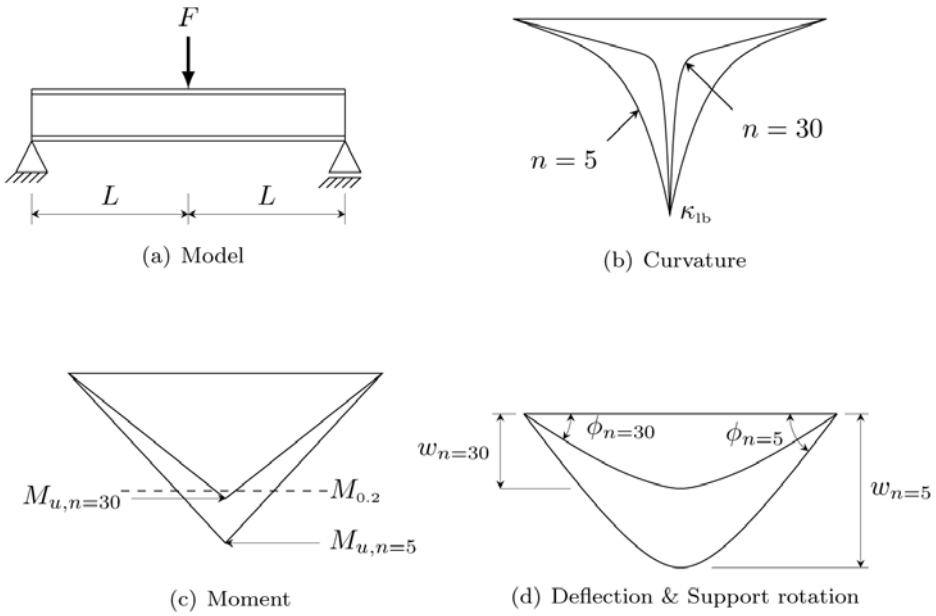

Figure 3 The effect of curvature localisation in a simply supported beam subjected to a concentrated force at its centre.

It was already shown in the previous section that the strain-hardening potential is increased at elevated temperatures. In this section it was found that effect of curvature localisation is less for materials with a greater degree of strain-hardening. For structures at elevated temperatures, the required ductility is thus less, and the influence of the required capacity part of equation 14 is a positive one. To quantify this effect, we will take a look at a more complex structure; the three span continuous beam, which is argued to be able to describe a wide range of structural types. Before this, the term curvature is introduced.

Curvature capacity

For an elastic perfect –plastic material, the (stable) rotation capacity is directly proportional to the rotation in the first appearing plastic hinge because all the plastic curvature is restricted to infinitely small hinges. This makes rotation capacity

a convenient way of describing the required ductility of a beam; it has a constant, material and cross-section independent, value for a given beam and load geometry, and it has a direct relationship to the curvature jump in the first appearing plastic hinge.

For round-house materials, this is no longer the case. It is exceeding a certain maximum curvature with associated cross-sectional plate strains which leads to local buckling to occur. The plastic deformation capacity is thus expressible by a curvature *capacity*, which is a cross-sectional property only.

The *required* curvature for a certain beam and load geometry is, for round-house materials, not an exclusive beam/load combination property, but also dependent on the strain-hardening potential of the alloy through the effect of curvature localisation; beams with less localized hinges require a lower maximum curvature. A way of comparing between bending members of equal ductility demand is the rotation capacity R_κ which is defined as

$$R_\kappa \equiv \frac{\kappa_{lb}}{\kappa_{0.2}} - 1 = \frac{\varepsilon_{lb}}{\varepsilon_{0.2}} - 1, \tag{18}$$

where the strains ε_{lb} and $\varepsilon_{0.2}$ are according to the most buckle sensitive plate of the cross-section.

Curvature distribution in a 3-span continuous beam

To study the required rotation capacity of real life structures, a model structure is required which needs multiple plastic hinges to develop before collapse occurs. A versatile type of structure, capable of simulating a wide range of structures is the 3-span continuous beam of figure 4.

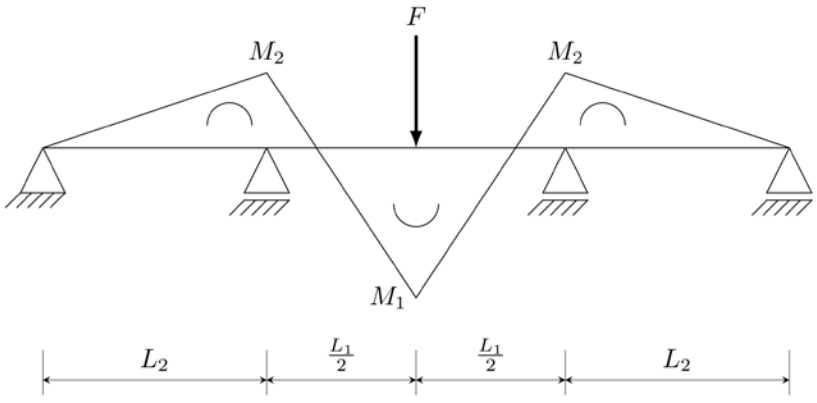

Figure 4 The elastic moment distribution due to a single concentrated force at the centre of the middle beam.

In figure 4, the elastic moment distribution due to a single concentrated force at the centre of the middle beam is drawn. The ratio between the elastic moments M_1 and M_2 is identical to the ratio between the rotations in the first occurring plastic hinge to the second, in case all rotations are thought restricted to plastic hinges. The ratio $|M_1/M_2|$ is therefore expected to have an approximately linear relation to the required rotation capacity. The ratio $|M_1/M_2|$ itself is a function of the geometry, and can be modified by changing the ratio between the lengths of the centre and the side span through

$$\left|\frac{M_1}{M_2}\right| = \frac{1}{\frac{3}{4}\frac{L1}{L2}} + 1\,. \tag{19}$$

Similar equations where made for other structural types, and through the $|M_1/M_2|$ ratio we can represent them all. A numerical procedure is employed to derive the moment and curvature distribution of the before mentioned 3-span continuous beam, based on equation 5. When we vary the ratio $|M_1/M_2|$, the required rotation capacity R reacts approximately linear as predicted. This is shown in figures figure 5 (a) and (b). There appears to be little influence of the exponent n or the geometrical shape factor a_0 (a geometrical shape factor of 1.15 is a typical value for an I - profile and 1.5 for a solid beam).

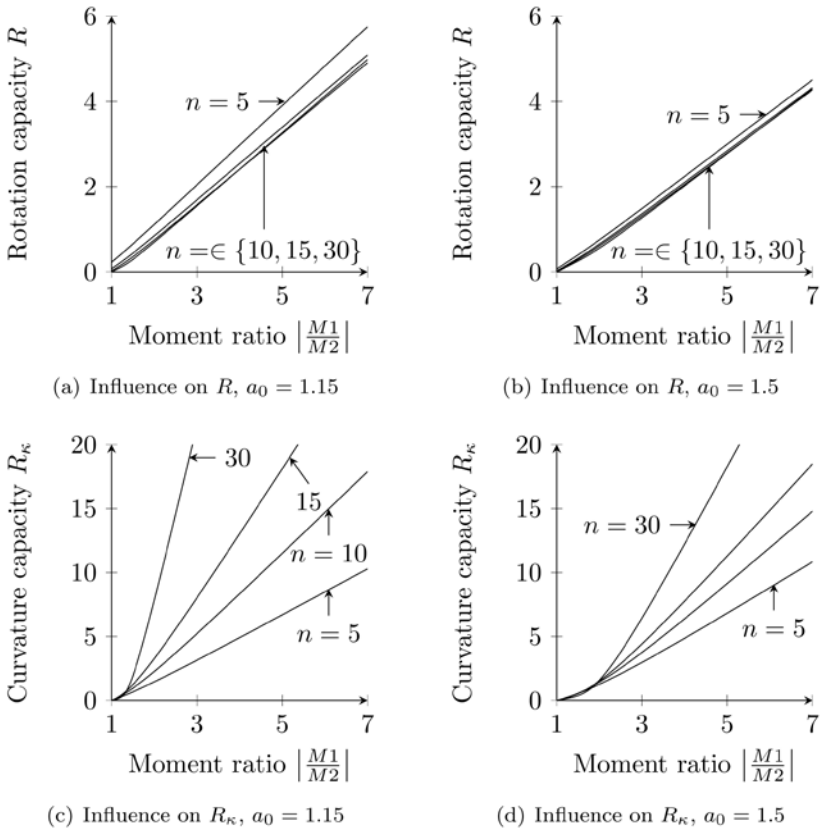

Figure 5 The required rotation capacity (a and b) and curvature capacity (c and d) for a symmetric 3 span beam with a concentrated force at its centre with a varied middle to side span ratio expressed in terms of the ratio between the resulting elastic moments.

A different picture arises when we do not look at the *rotation* capacity R_0, but rather at the *curvature* capacity R_κ. Figures 5(c) and (d), show the same results as in figures 5(a) and (b), but now in terms of the curvature capacity. A distinct influence of the strain-hardening potential is present, especially for the more optimized cross-sectional shapes as common for aluminium design and indicated with a low value for the generalized shape factor a_0. Because the curvature is less localised for (warmer) alloys with greater strain hardening potential, a lower maximum curvature is required for a plastic mechanism to form.

Example

To demonstrate the effect this has, we can take a look at figure 5(a) and lookup the $|M_1/M_2|$ ratio belonging to a stable rotation capacity of R_0=3 as specified by [3]. The maximum $|M_1/M_2|$ is equal to approximately 4. Aluminium alloy 6060-T66 has a minimum quoted value of n=16 at room temperature, and this is reduced to n_θ=5 at a temperature of 350°C. If we then look up the curvature capacity requirements for $|M_1/M_2|$ =4 in figure 5(c), the curvature requirement is reduced from $R_\kappa \approx 13$ to $R_\kappa \approx 5$ as the temperature is increased from room temperature to 350°C. Trough equation 14 and 18, it can then be calculated that the limit for the b/t ratio β is increased by 53% due to the diminished ductility demand, and a further 42% due to the increased k-part of equation 14. These numbers are obtained for the analytical form of equation 12. If we use the empirical constants C_1 and C_2 equal to 2.28 and 0.16, respectively, and solve the equations iteratively, a similar increase is observed. Then the b/t limit for a class 1 internal plate of 6060-T66 is equal to 12.2, which is increased to 17.5 at 350°C due to the decreased ductility demand. The increased stiffness over strength ratio at elevated temperatures further increases this limit to 24.9, which is actually higher than the limit for class 3 at room temperature.

Conclusions

An explorative study has been performed to investigate the potential for a cross-sectional classification system for beams in fire that better reflects the actual behaviour of such beams in practice as compared to the current design rules as given in the Eurocode for fire design [4]. It has been found that such potential exists and a simple equation is given to increase the geometric limits of class 2 and 3 sections, such that beams may be considered to be of a higher class in fire design. This is caused by the stiffness decreasing more slowly at an increase in temperature than the strength.

The rotational capacity requirements of class 1 sections have been investigated and it has been found that the curvature capacity demand is decreased at elevated temperatures due to the increase in strain-hardening potential and the decrease in curvature localisation. At the same time the curvature resistance is actually increased due to the increase in stability, which is again caused by the stiffness decreasing more slowly at an increase in temperature than the strength. Cross-sections that are of class 2 or higher at room temperature may thus be able to sustain sufficient plastic deformation to allow a plastic calculation according to the rules of class one as defined by [3].

Acknowledgement

This research was carried out under project number M81.1.108306 in the framework of the Research Program of the Materials innovation institute M2i (www.m2i.nl).

Nomenclature

ε	Strain
$\varepsilon_{0.2}$	Strain at the 0.2% proof stress
κ	curvature
σ	Stress
ν	Poisson's ratio
α_0	Geometrical shape factor (W_{pl}/W_{el})
b	Plate width
$f_{0.2}$	0.2% proof stress
$M_{0.2}$	Conventional elastic moment
M_1	Elastic moment at the place of the first yielding plastic hinge(s)
M_2	Elastic moment at the place of the yielding of a second (set of) plastic hinge(s)
M_u	Ultimate moment
M_{rd}	Design value for moment resistance
n	exponent in Ramberg-Osgood equation, expressing strain-hardening ability
R	Rotation capacity
R_0	stable rotation capacity
R_κ	Curvature capacity
t	Plate thickness
W_{el}	Elastic section modulus

Bibliography

[1] M. Cappelli, A. De Martino, F. M. Mazzolani, Ultimate bending moment evaluation for aluminium alloy members. In: R. Narayanan (Ed.), Proceedings of the international conference on steel and aluminium structures, Cardiff, UK, 8-10 July 1987, Elsevier Applied Science publishers, Essex, United Kingdom, 1987, volume: Aluminium structures pp. 126-134 ISBN: 1-85166-121-2

[2] G. De Matteis, R. Landolfo, M. Manganiello, A new classification criterion for aluminium cross-sections. In: G. J. Hancock, M. A. Bradford, T. J. Wilkinson, B. Uy, K. J. R. Rasmussen (Eds.), Proceedings of the international conference on advances in structures (ASSCCA '03), Sydney, Australia, 22-25 June 2003, A.A. Balkema, Lisse, the Netherlands, 2003, pp. 433-441. ISBN:90-5809-588-6

[3] EN 1999-1-1, Eurocode 9: Design of aluminium structures - Part 1-1: General structural rules, European Committee for Standardization (CEN), Brussels, Belgium, 2007

[4] EN 1999-1-2, Eurocode 9: Design of aluminium structures - Part 1-2: Structural fire design, European Committee for Standardization (CEN), Brussels, Belgium, 2007

[5] C. Faella, F. M. Mazzolani, V. piluso, G. Rizzano, Local buckling of aluminium members: testing and classification, Journal of Structural Engineering. 126 (2000) 3, pp. 353-360, DOI:10.1061/(ASCE)0733-9445(2000)126:3(353)

[6] S. Lundberg, Background document: Classification of cross-section classes in fire design, European Committee for Standardization (CEN), Brussels, Belgium, 2003, CEN/TC 250/SC 9/PT Fire/N-26, URL: http://www.eurocodes.fi/1999/1999-1-2/background/CEN_TC25_SC9.pdf (Retrieved March 1, 2010)

[7] J. Maljaars, F. Soetens, H. H. Snijder, Local buckling of slender aluminium sections exposed to fire, Journal of Structural Engineering 136 (2010) 1, pp. 66-75. DOI: 10.1061/(ASCE)ST.1943-541X.0000091

[8] M. Manganiello, G. De Matteis, R. Landolfo, Inelastic flexural strength of aluminium alloys structures, Engineering Structures. 28 (2006) 4 pp. 593-608. DOI: 10.1016/j.engstruct.2005.09.014

[9] F. M. Mazzolani, C. Faella, V. Piluso, G. Rizzano, Experimental analysis of aluminium alloy SHS-member subjected to local buckling under uniform compression. In: E. de M. Batista, R. C. Batista (Eds.), Stability problems in designing, construction and rehabilitation of metal structures: proceedings of the 5th International Colloquium on Structural Stability, SSRC Brazilian Session, Rio de Janeiro, August 5-7 1996, COPPE/UFRJ, Rio de Janeiro, Brazil, 1996, pp. 475-488 ISBN: 85-285-0017-9, 978-85-285-0017-2

[10] L. A. Moen, Rotation capacity of aluminium alloy beams, PhD thesis, Norwegian University of Science and technology, Department of Structural Engineering, Trondheim, Norway, 1999 ISBN: 82-471-0365-6 ISSN(series):0802-3271